Universiteit
Leiden
The Netherlands

Superlattices in van der Waals materials: a low-energy electron microscopy study

Jong, T.A. de

Citation

Jong, T. A. de. (2022, November 3). *Superlattices in van der Waals materials: a low-energy electron microscopy study*. *Casimir PhD Series*. Retrieved from https://hdl.handle.net/1887/3485753

Version:	Publisher's Version
License:	Licence agreement concerning inclusion of doctoral thesis in the Institutional Repository of the University of Leiden
Downloaded from:	https://hdl.handle.net/1887/3485753

Note: To cite this publication please use the final published version (if applicable).

2

Low Energy Electron Microscopy

The upside is: LEEM is sensitive to every tiny effect.
The downside is: LEEM is sensitive to each and every tiny effect.

2.1 INTRODUCTION

In this thesis, an Aberration Correcting Low Energy Electron Microscope (AC-LEEM) is used to image the structure of different Van der Waals materials. As the name suggests, LEEM uses electrons with low kinetic energy, typically just a few electronvolts.

Electrons are commonly used in microscopy instead of photons to obtain a resolution higher than the diffraction limit of (visible) light. Even at low kinetic energies the electron wavelength is much smaller than visible light photons and typically smaller than atomic distances in the sample.[1] Therefore, plane waves of electrons will diffract off the atomic lattice, forming multiple diffracted beams containing information about the atomic lattice itself.

Conventional electron microscopes, such as a Scanning Electron Microscope (SEM) or Transmission Electron Microscope (TEM), use a high energy electron beam and form an image with transmitted electrons, reflected electrons or secondary electrons, which are kicked out by the incoming beam. However, using high energy electrons has a significant downside: it generally damages the samples, significantly limiting the time that a sample can be imaged.

In contrast, most samples measured in LEEM can be imaged for hours or even days on end, without any significant damage to the sample. Furthermore, the low penetration depth of electrons at these low energies makes LEEM very surface-sensitive and the energy dependent reflectivity contains information about the three-dimensional atomic structure of the sample surface.

A LEEM setup is significantly different from what is used for TEM and SEM, and in some ways more similar to a conventional light microscope. To achieve the low interaction energies, the electrons in the microscope are, just like photons in a (conventional) light microscope, reflected off the sample surface. This reflection is enabled by an electric field which decelerates the electrons before the sample and reaccelerates them after reflection. Another aspect where LEEM is similar to a light microscope, is that the sample is illuminated by a broad beam (although of electrons instead of photons). Thus the image is created in one go, instead of built up pixel by pixel by scanning a beam as is done in SEM (and high resolution scanning TEM).

In this chapter, a brief introduction of the various principles of LEEM imaging used in this thesis is given. For the sake of brevity it does not cover all possibilities and details, but more elaborate explanations are available elsewhere [22–24].

The LEEM used in this work is the ESCHER LEEM at Leiden University. It is a SPECS P90 based system based on the aberration correcting design by R.M. Tromp [25–27].

2.2 IMAGING

To obtain a LEEM image in the ESCHER LEEM, electrons are first emitted from a cold field-emission gun, the electron source (at the top of Figure 2.1). To be able to form this beam and steer the electrons they are accelerated to a kinetic energy of 15 keV, as low energy electrons are too sensitive to changing stray fields (both electric and magnetic).

[1] However, LEEM can use energies so small that the electron wavelength is larger than atomic structures. The cross-over lies around 30 eV

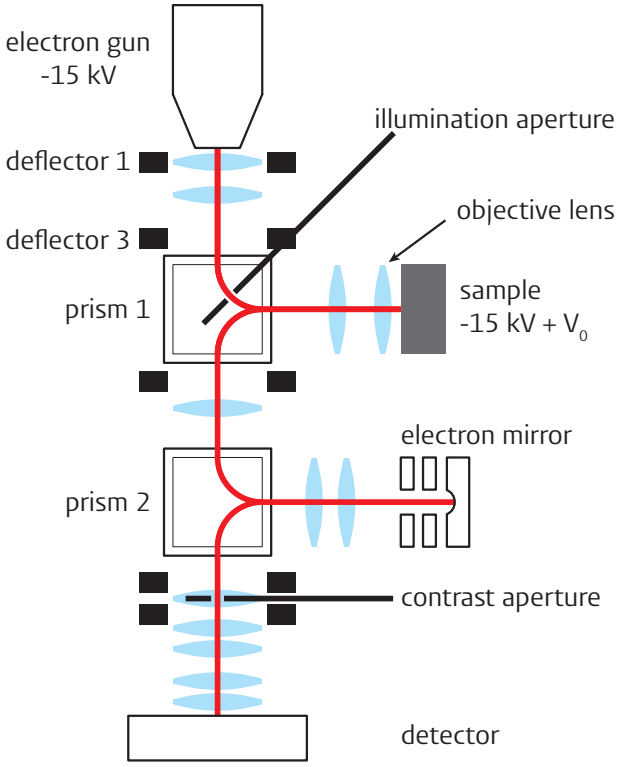

Figure 2.1: *Diagram of an aberration correcting LEEM as used throughout this work: the SPECS P90 based ESCHER LEEM at Leiden University with 90° deflecting prisms and an electron mirror for aberration correction. The path of the electron beam is indicated in red, the electron lenses in light blue and the most relevant deflectors with black rectangles.*

The electrons are shaped into a consistent beam using deflectors 1 and 3 and a pair of electron lenses[2].

To separate the incoming and reflected beams, the electrons, depicted in red, first go through a prism: a perpendicular magnetic field that bends the path of the electrons towards the sample due to the Lorentz force. The sample is mounted on a sample stage and is elevated to an electric potential of $-15\,\mathrm{kV} + V_0$. In this way, the electric field between the objective lens (which is at ground potential, just like the rest of the microscope) and the sample decelerates the electrons to a kinetic *landing energy* $E_0 := eV_0 + (\Phi_g - \Phi_s)$ before interacting with the sample. Here, $(\Phi_g - \Phi_s)$ is the difference in work function between the electron gun and the sample, such that the electrons interact with the sample itself for $E_0 > 0$. The landing energy E_0 can be changed by simply changing the potential offset V_0, i.e. the voltage applied to the sample.

The electrons form an illuminated area on the sample with a diameter of several micrometres. To align the sample with respect to the incoming electron beam and to access a larger area of the sample, it is mounted on a five axis movable sample stage that is moved using micro-actuators [28]. After interacting with the sample, the same electric field between sample and objective lens reaccelerates the electrons towards the prism.

[2] More deflectors are present in the LEEM (including deflector 2), but are not detailed here where they are not relevant to the working principles

Just like in a light microscope, the reflected (electron) waves now contain information about the sample in two complementary ways: in each *image plane* the intensity at a position corresponds to the reflectivity of the sample at the corresponding position and electrons emitted at all angles from this position are collected at the same position. Inversely, in each *diffraction plane* (or back-focal plane), the intensity at a position corresponds to the average reflectivity of the sample at a corresponding **angle**, with all electrons emitted under this angle at all illuminated positions of the sample collected at the same point. The coordinates in the diffraction plane are the in-plane momenta of the electrons as they leave the sample. Thus, the different diffracted beams are (spatially) separated as spots in diffraction planes (As visible in Figure 2.2**a**). As the electrons propagate through the microscope and get focused and refocused by the lenses, the beam alternately passes through several image and diffraction planes. It is worth noting that the image plane and diffraction plane exhibit *duality* properties in the full mathematical sense: applying the transformation from image to diffraction plane, (which corresponds to a Fourier transform) twice yields an image plane again (and vice versa) [3]. However, this (Fourier) transformation mixes intensity and phase information of a real space plane to both phase and intensity in a diffraction plane (and vice versa), while only intensities can be measured.

The aim of the rest of the microscope is to capture the relevant parts of this information using a detector. The prism directs the returning electrons down into the imaging column. In principle these electrons can now directly be used to create an image of either the image plane or the diffraction plane using an imaging electron detector. However, the resolution would be limited by the aberrations of the objective lens: it is impossible to design an aberration-free electron lens. Fortunately, it is possible to create an *electron mirror* with aberrations that can be tuned to cancel the worst, i.e. the leading orders, aberrations introduced by the objective lens. Therefore the electrons go through a second, identical prism (prism 2 in Figure 2.1) that directs them to the electron mirror. The mirror consists of three annular focusing electrodes (dioptric elements) and a solid spherical concave electrode (catoptric element) that controls the shape of the reflecting equipotential. This catadioptric mirror acts as a 1:1 transfer lens for both image and diffraction planes, with the incident and reflected images coinciding in the object plane, and the diffraction pattern located at the symmetry (i.e. reflection) plane. By tuning the relative potentials of the mirror electrodes, the aberrations of the mirror are set to cancel the aberration of the objective lens up to third order spherical aberration and second-rank chromatic aberration [24].

The reflected, and now aberration-corrected, electrons are once again deflected by prism 2 towards the projector. The projector consists of a set of deflectors and five lenses that create a magnified image on a pixelated detector generating a digital image.

The detector can switch easily between imaging the image plane and the diffraction plane, as the strength of the electron optical lenses in the projector (as for any electron-optical lens) can be changed quickly by changing the currents that determine the electromagnetic fields that form the lens. Imaging the diffraction plane is refered to as **Low-Energy Electron Diffraction** mode (LEED, or even VLEED, where V stands for 'Very', as the energies can be lower than in simpler, dedicated LEED instruments).

[3] See e.g. Ref. [22] for a nice visualization.

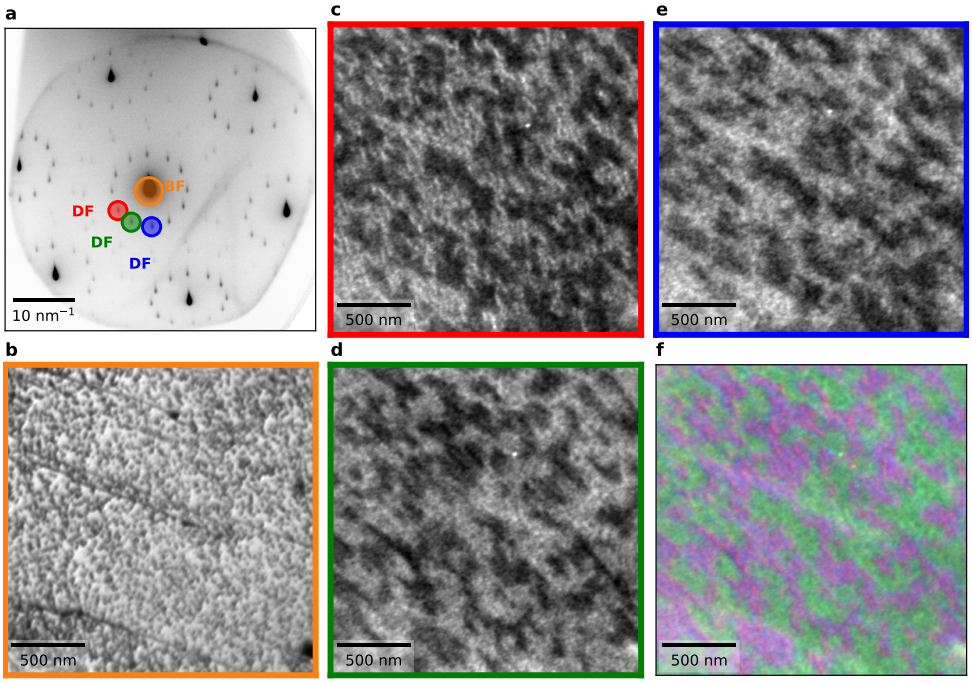

Figure 2.2: ***a,*** *Diffraction pattern of TaS_2, which has a twinned $\left(\sqrt{13}\times\sqrt{13}\right)R13.9°$ CDW reconstruction visible as extra spots (Explored in detail in Chapter 8). Aperture positions for Bright Field imaging and Dark Field imaging on 3 CDW spots are indicated with circles.* ***b,*** *Using a contrast aperture around the specular reflection spot yields a BF-LEEM image.* ***c,*** *Using a contrast aperture around any other spot (position indicated in* ***a****) yields a DF-LEEM image highlighting the areas where the (CDW) periodicity corresponding to the spot occurs on the sample.* ***d,e,*** *Using an aperture around different diffraction spots can yield an inequivalent DF-LEEM image.* ***f,*** *The (gray scale) DF-LEEM images in* ***c-e*** *can be combined into the color channels of a color image to create a composite dark field image. In this specific example, red and blue are equivalent, therefore the contrast in this case is mainly purple versus green.*

The aberration correction significantly increases the best achievable resolution in LEEM mode to a line resolution of lower than 6 nm (achieved on 2-on-2 Twisted bilayer graphene, see Figure 6.2), i.e. parallel lines with a spacing of less than 6 nm can be resolved. In terms of an often used 20%/80% criterion this corresponds to a resolution of about 1.2 nm. Despite this resolution improvement, the resolution is still not sufficient to directly image individual atoms using LEEM mode. In the next section, we explain how we instead rely on various imaging modes using LEEM and LEED modes in conjunction to extract information about the atomic lattice.

2.3 IMAGING MODES

To aid extracting specific information from the electron wavefront, several different imaging modes can be used, by restricting the electron beam with apertures that are mounted

at image planes and diffraction planes at several places in the microscope. The most important aperture is the *contrast aperture*, located in a diffraction plane in the projector, as indicated in Figure 2.1. Its name is derived from the fact that it fits in a diffraction plane and therefore can be used to select electrons leaving the sample within a specific range of angles to increase image contrast by blocking out all other electrons. This in particular includes non-elastically reflected electrons and secondary electrons, which leave the sample with a lower kinetic energy and are therefore deflected more strongly by the prisms.

If the contrast aperture is used to select the specularly (i.e. zeroth-order diffraction) reflected electrons, the resulting real space image is a **Bright Field** (BF-LEEM, Figure 2.2**b**) image. If the contrast aperture is used to select a diffracted beam, it is a **Dark Field** (DF-LEEM, Figure 2.2**c-e**) image. Such a Dark Field image has intensity only in positions on the sample that emit electrons under the specific angles selected by the position of the contrast aperture, e.g. positions on the sample that exhibit a periodicity of atoms that will emit a diffracted beam under that angle.

The second aperture relevant to this thesis is the *illumination aperture*. It slides into an image plane in the top half of prism 1, indicated in Figure 2.1. As the name suggests, it restricts the extent of the electron beam going towards the sample, limiting the area of the sample which is illuminated with electrons down to an area of a few hundred nanometre across. This enables **μLEED**, where a diffraction pattern can be obtained of a specific area of the sample. As the same area can be imaged in LEEM mode and this illuminated area is much smaller, this enables more detailed study of diffraction patterns than in a traditional LEED setup.

2.4 LEEM AND LEED SPECTROSCOPY

Both real space images and diffraction images can be obtained as a function of E_0 to obtain spectroscopic information. These spectroscopic datasets are traditionally labeled LEEM-I(V) and LEED-I(V) respectively, as the **I**ntensity is measured as a function of $\mathbf{V}_0$. (Not to be confused with a Current–Voltage measurement in transport physics!) However, for properly calibrated datasets (See Chapter 3), this is a bit of a misnomer, as the electron reflectivity as a function of E_0 is measured. In this thesis, such measurements are therefore referred to as spectroscopic LEEM and spectroscopic LEED data.

For spectroscopic LEEM data, consisting of real space images, spectra from different areas of the sample can be obtained by measuring the average intensity of such an area for each obtained image. For diffraction patterns, equivalently, spectra of intensity as a function of E_0 for different diffracted beams can be measured. Note again the duality between diffraction and real space: in BF/DF-LEEM spectroscopy the diffraction spot selection is done using the contrast aperture during the measurement and the sample area is selected during data analysis, while in μLEED spectroscopy the area is selected using the illumination aperture and the diffraction spot is selected during data analysis.

The addition of spectral information to images greatly enhances which information can be extracted from the sample [24, 29]. The energy dependent reflectivity is very sensitive to the atomic structure of the sample surface, enabling finger printing of different surface structures to distinguish them. By comparing measured spectra to calculations of the low energy electron reflectivity for different atomic structures, identification of

precise atomic structures is possible. Note that the inverse, *directly* deducing or calculating the atomic structure from LEED spectra is impossible, so to extract a precise atomic structure, the positions of the atoms have to be iteratively refined, calculating reflectivity from every configuration until an optimum is achieved.

The computational techniques were originally developed for traditional LEED, which uses slightly higher landing energies. They were therefore optimized by using a simplified model, making such calculations inaccurate for $E_0 \lesssim 80$ eV. Increasingly, it has become possible to calculate low energy electron reflectivity even for the very low energies occuring in LEEM by using ab-initio scattering calculations, essentially solving the full electron wave propagation problem, but computationally more expensive. Relevant for this thesis, it was for example shown that it is possible to count the number of Van der waals layers on a substrate [30, 31]. In this thesis, we will extend upon the possibilities to extract the relative positions of atoms in the Van der Waals layers by comparing to ab-initio calculations performed by Eugene Krasovskii.

2.4.1 FURTHER NOTES ON EXPERIMENTS

Both spectroscopic measurement methods, LEEM and (V)LEED, can obtain a spectrum of a specific diffraction spot as a function of energy. In practice, whether a dataset comparing different areas on the sample or a dataset with multiple diffraction spots of the same area is needed determines whether a dataset is measured in LEEM or in LEED mode. It is however worth noting that the obtained spectra are not fully equivalent. The selection of an area in an image or diffraction pattern during data analysis can be more precise, as it is not restricted by the physical size of apertures. A further subtle difference is that if the intensity is low compared to other areas or diffracted beams on the detector, the measured contrast can be limited by the dynamic range of the detector, even in high dynamic range imaging mode as detailed in Chapter 3.

All LEEM images and spectroscopic LEEM data in this thesis use a contrast aperture and are therefore either BF-LEEM or DF-LEEM data.

Beyond varying E_0, other parameters can be varied as well, for example the sample position in a μLEED measurement for so-called *scanning* μLEED [32, 33], or the in-plane momentum for Angular Resolved Reflective Electron Spectroscopy [34]. These combined techniques play however no significant role in this thesis.

The next chapter will focus on extracting spectra from the raw data, the necessary steps before we can use such data for material science.

REFERENCES

22. J. Kautz. *Low-energy electron microscopy on two-dimensional systems : growth, potentiometry and band structure mapping* PhD thesis (Leiden University, 2015). https://hdl.handle.net/1887/32852.

23. T. A. de Jong. *Stacking domains in bilayer Van der Waals materials* MSc thesis (Leiden University, 2017). https://hdl.handle.net/1887/52790.

24. R. Tromp. In *Springer Handbook of Microscopy* (eds P. W. Hawkes & J. C. H. Spence) 565–604 (Springer International Publishing, Cham, 2019). doi:10.1007/978-3-030-00069-1_11.

25. R. Tromp, J. Hannon, A. Ellis, et al. A new aberration-corrected, energy-filtered LEEM/PEEM instrument. I. Principles and design. *Ultramicroscopy* **110,** 852–861. doi:10.1016/j.ultramic.2010.03.005 (2010).

26. S. Schramm, J. Kautz, A. Berghaus, et al. Low-energy electron microscopy and spectroscopy with ESCHER: Status and prospects. *IBM Journal of Research and Development* **55,** 1–1. doi:10.1147/JRD.2011.2150691 (2011).

27. R. M. Tromp, J. B. Hannon, W. Wan, A. Berghaus & O. Schaff. A new aberration-corrected, energy-filtered LEEM/PEEM instrument II. Operation and results. *Ultramicroscopy* **127,** 25–39. doi:10.1016/j.ultramic.2012.07.016 (2013).

28. A. W. Ellis & R. M. Tromp. A versatile ultra high vacuum sample stage with six degrees of freedom. *Review of Scientific Instruments* **84,** 075112. doi:10.1063/1.4813739 (2013).

29. J. I. Flege & E. E. Krasovskii. Intensity-voltage low-energy electron microscopy for functional materials characterization. *Physica Status Solidi - Rapid Research Letters* **8,** 463–477. doi:10.1002/pssr.201409102 (2014).

30. H. Hibino, H. Kageshima, F. Maeda, et al. Microscopic thickness determination of thin graphite films formed on SiC from quantized oscillation in reflectivity of low-energy electrons. *Physical Review B* **77,** 075413. doi:10.1103/PhysRevB.77.075413 (2008).

31. T. A. de Jong, J. Jobst, H. Yoo, et al. Measuring the Local Twist Angle and Layer Arrangement in Van der Waals Heterostructures. *physica status solidi (b)* **255,** 1800191. doi:10.1002/pssb.201800191 (2018).

32. K. L. W. Lau, K. M. Yu, D. Luo, R. S. Ruoff & M. S. Altman. High throughput scanning μLEED imaging of surface structural heterogeneity: Defective graphene on Cu(111). *Ultramicroscopy* **200,** 67–72. doi:10.1016/j.ultramic.2019.02.015 (2019).

33. V. A. E. C. Janssen. *Electronic Properties of (Pseudo-) Two-Dimensional Materials* PhD thesis (2020). doi:10.4233/UUID:0C9F992C-7390-4D8F-AA6D-D89F0E7866A0.

34. J. Jobst, A. J. H. van der Torren, E. E. Krasovskii, et al. Quantifying electronic band interactions in van der Waals materials using angle-resolved reflected-electron spectroscopy. *Nature Communications* **7,** 13621. doi:10.1038/ncomms13621 (2016).